A Comparison of Active and Passive Methods for Control of Hypersonic Boundary Layers on Airbreathing Configurations

Scott A. Berry and Robert J. Nowak
NASA Langley Research Center, Hampton, VA

Abstract

Active and passive methods for control of hypersonic boundary layers have been experimentally examined in NASA Langley Research Center wind tunnels on a Hyper-X model. Several configurations for forcing transition using passive discrete roughness elements and active mass addition, or blowing, methods were compared in two hypersonic facilities, the 20-Inch Mach 6 Air and the 31-Inch Mach 10 Air tunnels. Heat transfer distributions, obtained via phosphor thermography, shock system details, and surface streamline patterns were measured on a 0.333-scale model of the Hyper-X forebody. The comparisons between the active and passive methods for boundary layer control were conducted at test conditions that nearly match the nominal Mach 7 flight trajectory of an angle-of-attack of 2-deg and length Reynolds number of 5.6 million. For the passive roughness examination, the primary parametric variation was a range of trip heights within the calculated boundary layer thickness for several trip concepts. The prior passive roughness study resulted in a swept ramp configuration being selected for the Mach 7 flight vehicle that was scaled to be roughly 0.6 of the calculated boundary layer thickness. For the active jet blowing study, the blowing manifold pressure was systematically varied for each configuration, while monitoring the mass flow, to determine the jet penetration height with schlieren and transition movement with the phosphor system for comparison to the passive results. All the blowing concepts tested were adequate for providing transition onset near the trip location with manifold stagnation pressures on the order of 40 times the model static pressure or higher.

Introduction

Recently NASA refocused space access research into the Space Launch Initiative (SLI), which established the Next Generation Launch Technology (NGLT) program. The objective of NGLT is to advance the state-of-the-art in space transportation systems (STS) technologies for affordable and reliable transportation to and from earth orbit through development of innovative approaches and concepts for future missions of human and robotic exploration of space. A major component of NGLT is the advancement of rocket and air-breathing propulsion technologies: to lower the cost of proven rocket-powered systems, while developing and demonstrating the revolutionary air-breathing technologies of the scramjet engine. Since the advent of the National Aerospace Plane (NASP) program in the mid-80's, a scramjet powered vehicle has been a vision of affordable and rapid access to space. Scramjet powered vehicles scoop the oxygen required for fuel combustion from the atmosphere, reducing the tanking requirements, which can lead to improved payload capability. However the promise of scramjet as a propulsion system will be only an illusion until a flight program can conclusively demonstrate the technology. The Hyper-X program, a subset of NGLT, endeavors to provide a demonstration with a Mach 7 flight.

Conceptually, a scramjet-powered system appears very simple, with no moving parts required to provide flow compression and only fuel addition and ignition needed to provide thrust. However, the feasibility of just such a system has always been tied to the details of trying to integrate the engine to the airframe using innovative materials and structures to control the highly complex flow field while handling the high heat loads. For airframe-integrated scramjet engines, the forebody ahead of the inlet is designed to process and pre-condition the flow that will be ingested. As shown in Fig. 1, a full-scale air-breathing vehicle will likely have competing transition mechanisms in the forebody boundary layer that will naturally force turbulent flow ahead of the inlet, which is desirable as susceptibility to flow separations within the engine will be diminished. However, on a sub-scale vehicle such as the Hyper-X, the shortened forebody is likely to provide laminar flow to the engine, based on the Mach 7 trajectory. The Hyper-X program decided early in the design to utilize

Approved for public release; distribution is unlimited.

boundary layer trips to force turbulent flow on the forebody in order to properly scale the engine flight test results to future full-scale vehicles. Berry, et al. (2001) provides an overview of the experimental program that was set up to test and compare several passive trip concepts for the Mach 7 flight.

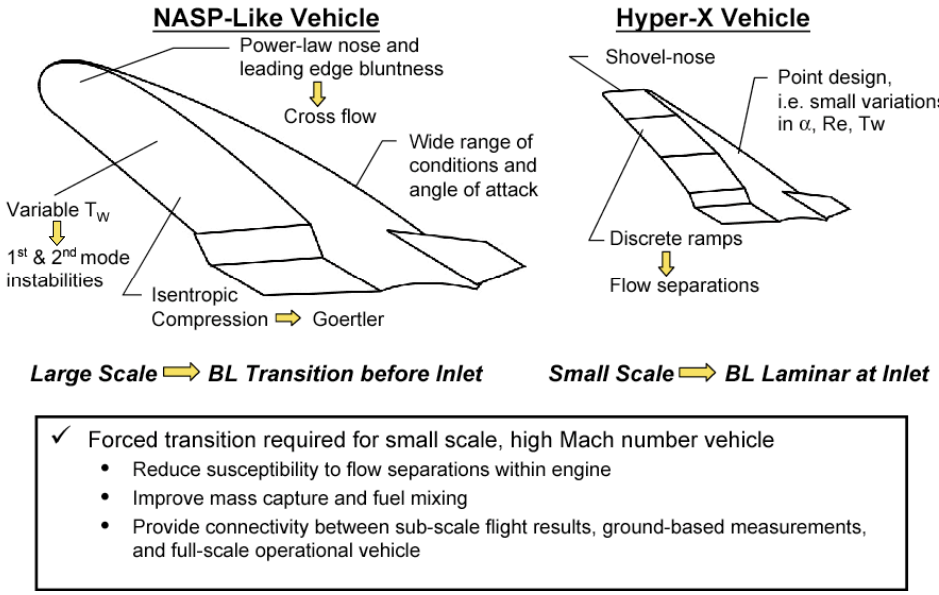

Figure 1: Transition mechanisms for airbreathing concepts.

A critical step in the design of hypersonic vehicles is to consider the effects of surface roughness on the boundary layer in order to determine the total heat load on the vehicle for sizing of the thermal protection system (TPS). Typically of interest is a determination of the various forms of roughness that can occur on the vehicle and an understanding of the critical roughness sizes that will allow as much laminar flow as possible in order to minimize the aeroheating to the vehicle. For instance, a reentry vehicle with an ablating TPS surface coating can develop a distributed and random surface roughness pattern, while a ceramic tile TPS can provide for specific discrete roughness sites due to slight misalignments of the tiles forming steps and/or gaps on the surface. As depicted in Fig. 2, wind tunnel experiments are conducted to simulate the expected roughness in hopes of determining the critical dimensions that will adversely affect the TPS design. For the Hyper-X vehicle, the reverse was required: a determination of the critical dimensions that will promote transition in a controlled manner. A wind tunnel program was implemented to screen and down select several passive discrete trip configurations resulting in an array of swept ramp vortex generators, shown in Fig. 3, being chosen for the Mach 7 flight, as detailed in Berry, et al. (2001). Since the time of these initial studies, additional tests have been performed to investigate the feasibility of implementing an active method of boundary layer control via steady mass addition (blowing) for use on subsequent flights. An active system offers the advantage of being able to tailor the amount of boundary layer control to the environment, essentially turning the system on only when needed (although there may a weight penalty associated with the additional system requirements). The present paper provides a status report of the results obtained to date on this exploratory investigation into using surface mass addition (also referred to as blowing) as a tripping device for future hypersonic airbreathing vehicles.

Three new active-trip screening tests, shown added to Table 1, have been completed in the LaRC 20-Inch Mach 6 and 31-Inch Mach 10 tunnels. The purpose of these tests was to investigate various methods for blowing on the Hyper-X forebody and to compare these results to the discrete roughness element results previously obtained. The present results utilize a common model and test technique to the published results used to establish the passive trip design for the Hyper-X Mach 7 flight vehicle. Test techniques that were utilized include thermographic phosphors (provides images of the global surface heating), schlieren (provides detailed shock shapes), and oil-flow (provides surface streamline information). The assembly and instrumentation for blowing was designed and built to fit within the space previously occupied by the passive

trip inserts with a minimum amount of modification to the existing model. The primary parametrics in these tests was a range of manifold pressures while monitoring of the total mass flow for the various blowing configurations at the nominal angle of attack ( ) of 2-deg, and a unit Reynolds number (Re) of 2.0 million per foot, with the inlet cowl door simulated in the open position. The blowing configuration parametrics, which consisted of 3 basic concepts (various arrangements of holes, two and three dimensional slots, and random porosity) for providing induced vorticity within the boundary layer, were selected to provide guidelines for development of an efficient trip design for the Hyper-X flight vehicle. Additional details of the previous passive roughness experimental results can be found in Berry, et al. (2000a and 2000b) and Calleja (2000). This report presents a comparison of the results from the current investigation into active methods to control the boundary layer to the earlier passive results.

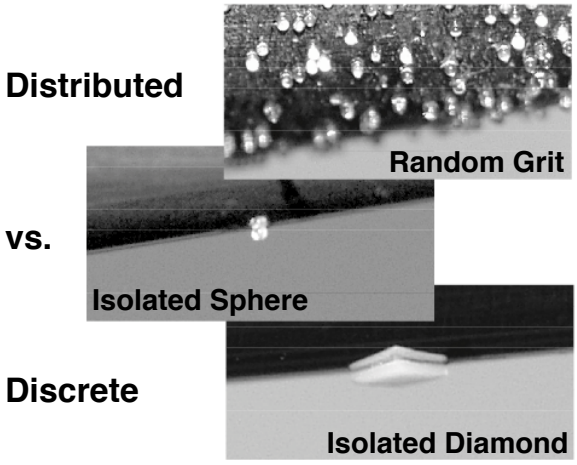

Figure 2: Classical methods for tripping boundary layers.

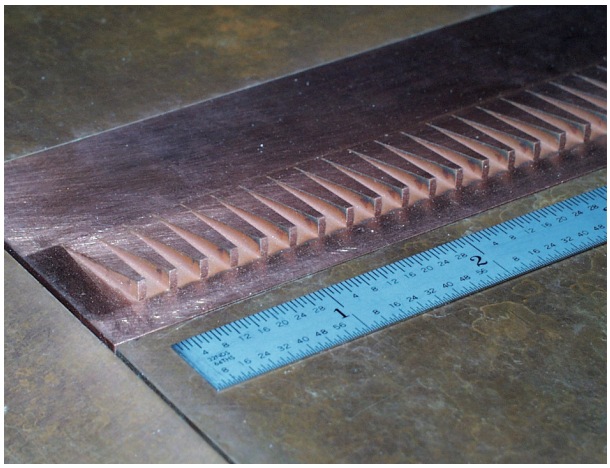

Figure 3. Close-up photograph of selected trip configuration scaled for Mach 7 flight conditions.

Hyper-X and Trip Design

The Hyper-X program (X-43A) is intended to flight test an operational airframe-integrated scramjet propulsion system at hypersonic conditions. Flights at Mach 7 and 10 are planned, details of which can be found in Rausch, et al. (1997a, 1997b) and McClinton, et al. (1998). The objective of this program is to obtain flight data on an autonomous hypersonic airbreathing propulsion system that is fully integrated with the vehicle airframe, thus validating/calibrating the experimental, numerical, and analytical methods that were used for design and flight performance prediction. As with all cutting-edge flight programs, numerous technologies had to be matured to acceptable levels in order to ensure program success. One such technology was the establishment of an efficient means for control of the boundary layer on the flight vehicle. To minimize susceptibility of the scramjet engine to shock-induced flow separations, and thus engine unstarts, the boundary layer approaching the inlet should be turbulent. Based on the current knowledge of boundary layer transition for slender, planar configurations at hypersonic flight conditions, an estimation of the location of natural transition on the Hyper-X forebody indicates that boundary layer trip devices are necessary to ensure a turbulent boundary layer at the inlet for both Mach 7 and 10 flights. Figure 3 provides a photograph of the final trip configuration and size selected for the Mach 7 flight.

As part of a fully integrated scramjet propulsion system, the Hyper-X vehicle windward forebody is designed to compress and process the flow going into the inlet. The windward forebody is approximately 6-ft long and is characterized by a thin leading edge (R_n = 0.03-in) and 3 flat ramps that provide a series of discrete, non-isentropic flow-compressions for the engine. While flying at the nominal angle of attack of 2-deg, the first forebody ramp provides an initial 4.5-deg of compression, followed by the second ramp with an additional 5.5-deg, and finally the third ramp with the final 3-deg of additional compression. Outboard of the flat ramps are the chines, which are designed to minimize three-dimensional effects and flow spillage. Ideally, the forebody would also provide a turbulent boundary layer for the inlet. A full-scale scramjet-powered vehicle, such as NASP or a similar derivative, would likely have sufficient forebody length to provide a naturally turbulent

boundary layer. Therefore, as a sub-scale vehicle, Hyper-X requires forced boundary-layer transition in order to properly scale the engine flight test results to a future full-scale vehicle. While the primary emphasis for the trips is to provide a turbulent boundary layer for the inlet, a secondary concern is whether a laminar separation at the end of the first ramp will promote lateral spillage of the forebody boundary layer away from the inlet, potentially reducing the mass capture and affecting performance. An analysis of the Hyper-X forebody using the hypersonic boundary layer transition criteria developed during the NASP program[1] suggests that the vehicle forebody will remain laminar during the flight. The results from this analysis are detailed in a Hyper-X Technical Note written by Dilley (1996). A boundary layer code was used to compute laminar values of Re_{θ}/M_e for a sharp nose wedge with 4.5-deg compression angle. The NASP sharp planar transition criterion of Re_{θ}/M_e = 305 was used to estimate the onset of transition. For an initial assessment, this sharp planar criterion was deemed acceptable, as nose bluntness has a stabilizing influence that would further delay transition onset (Stetson, 1984). Based on this initial estimate, transition will not occur on the first ramp prior to the compression corner. In fact, over 200% more running length is required for transition to occur on the first ramp based on the accepted criterion, which is beyond the inlet. Thus, without some sort of flow tripping device, the potential exists for a laminar separation at the first ramp break to generate some degree of lateral spillage. As for the question of transition prior to the inlet, the discrete compression corners will tend to promote transition, but to what extent is unclear. Very little ground based experimental data is available to provide guidance on forced transition through the use of discrete compression corners, and certainly less flight experience. To be conservative, the decision was made to force transition through the use of a passive (non-retractable) trip array on the first ramp to ensure, at the very least, turbulent flow into the inlet, and also provide some flow spillage relief at the first ramp break. Initial investigations into forced transition in hypersonic boundary layers utilized large spheres attached to the surface, as shown in Fig. 2. Recent work at LaRC provided the diamond configuration, also shown in Fig. 2, which appeared to be a more efficient trip mechanism. The work to define the passive trip array for the flight vehicle essentially was an effort to further optimize the vortex generating ability of the diamond configuration and at the same time reduce the inherent parasite drag of the final trip design selected and shown in Fig. 3.

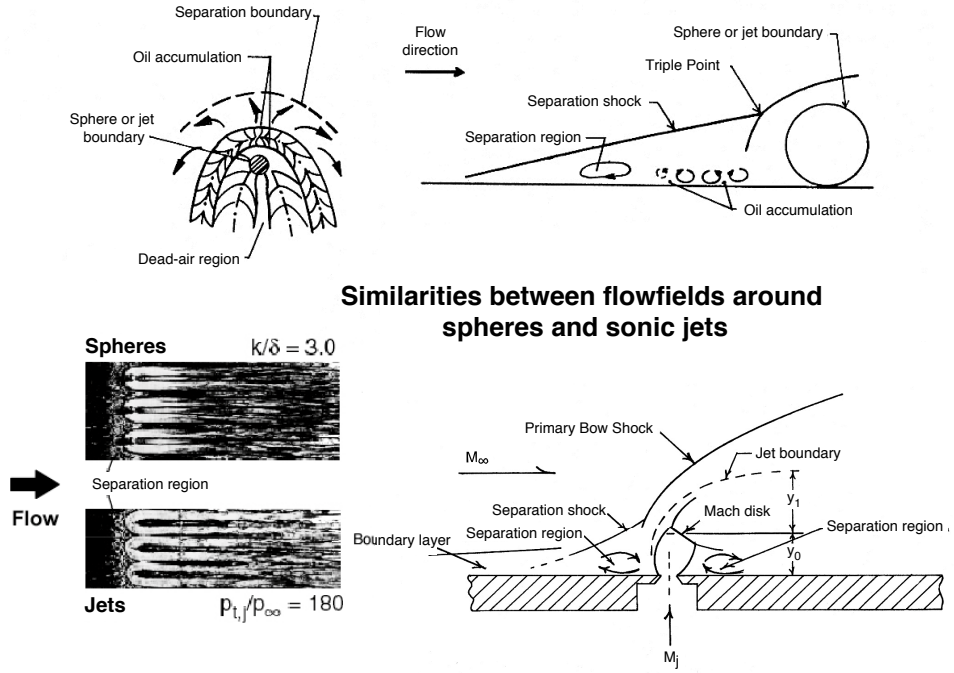

Figure 4: Previous active vs. passive trip research from Stone and Cary (1972).

[1] While much of the NASP documentation is currently still classified, the boundary layer transition criteria developed during NASP are considered unclassified. Lau and Vaporean (1992) discuss the NASP transition database.

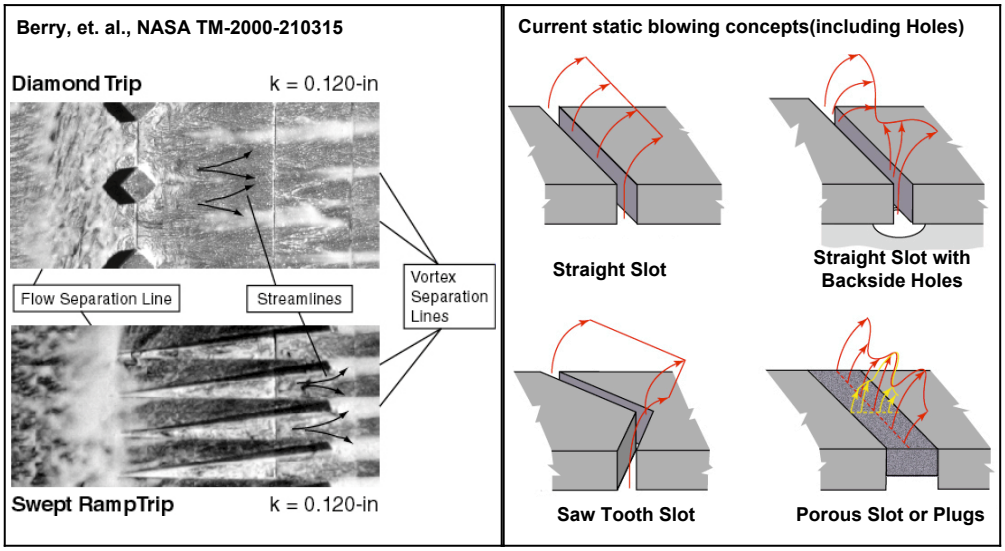

Figure 5: Current active vs. passive trip research.

Sonic jets have been studied for many years for use as vehicle attitude control devices. Many of these early studies also recognized that these devices were able to induce vorticity and thus transition in the boundary layer. Stone and Cary (1972) investigated discrete sonic jets as boundary layer trips and found that the tripping ability of active blowing of this type was in many ways analogous to the results obtained from passive spheres, as shown in Fig. 4. While the previous work reported by Berry, et al. (2001) tried to improve upon the trip effectiveness of spheres for use in a flight vehicle program, the current work attempts to re-investigate blowing as a trip mechanism to see if further improvements are possible. As shown in Fig. 5 for the earlier work, surface streamline directions indicate induced vorticity from the passive trip arrays. The current blowing or mass addition concepts were conceived to provide an alternative method for inducing vorticity. Figure 6 provides the specific configurations tested, which includes various hole arrays, straight and saw-tooth slots, concepts utilizing porous inserts, and several backing plates designed to periodically obstruct the holes or slots. The backing plates are intended to provide for greater parametric variation in both the number of holes that are employed for any given run and to introduce three-dimensionality to the two-dimensional straight slot configuration. The current study is an exploratory investigation into the potential use of an active blowing system for control of the boundary layer and to compare the results to that obtained previously using passive roughness elements.

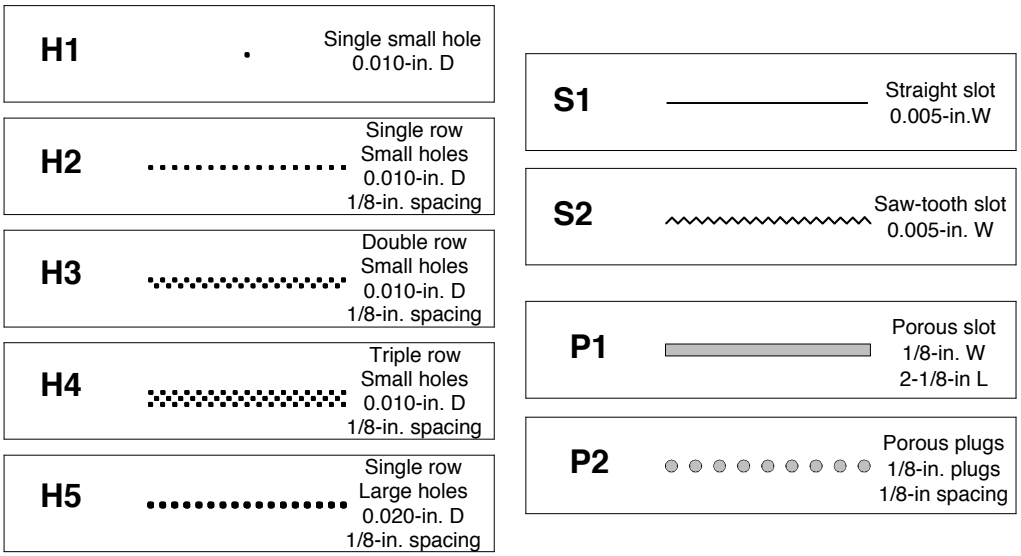

Figure 6: Configurations tested in the current research

Experimental Methods

Test Facilities

The Hyper-X forebody model has been tested in both the 20-Inch Mach 6 Air and the 31-Inch Mach 10 Air Tunnels of the LaRC Aerothermodynamic Laboratory (LAL). The LAL facilities are conventional blow-down tunnels that utilize dried, heated, and filtered air as the test gas. Detailed descriptions of these facilities and their associated instrumentation are found in Miller (1990) and Micol (1998). Typical operating conditions for the LaRC 20-Inch Mach 6 Air Tunnel are stagnation pressures ranging from 30 to 500 psia, stagnation temperatures from 410 to 500°F, and free stream unit Reynolds numbers of 0.5 to 7.8×10^6/ft. A two-dimensional, contoured nozzle is used to provide a nominal freestream Mach number of 6. The test section is 20.5 by 20 inches. A bottom-mounted model injection system inserts models from a sheltered position to the tunnel centerline in less than 0.5-sec. Run times of up to 15 minutes are possible with this facility, although for typical heat transfer and flow visualization tests, only a few seconds are required. Optical access to the model was viewed through a high-quality window on the top of the tunnel for phosphors and oil-flow, while high-quality windows on the side provided schlieren access. Typical operating conditions for the LaRC 31-Inch Mach 10 Air Tunnel are stagnation pressures ranging from 350 to 1450 psia and a stagnation temperature on the order of 1350°F, which yields freestream unit Reynolds numbers of 0.5×10^6/ft to 2.2×10^6/ft. The tunnel has a closed 31- by 31-in. test section with a contoured three-dimensional water-cooled nozzle to provide a nominal Mach number of 10. A hydraulically operated side-mounted model injection mechanism injects the model into the flow in 0.6 seconds. The maximum run time for this facility is approximately 2 minutes; however, only 5 seconds is typically required for transient heat transfer tests. Optical access to the model mechanism for both phosphors and oil-flow is viewed through high-quality top and side windows.

Test Techniques

A two-color, relative-intensity phosphor thermography system is currently being utilized for aeroheating tests in LAL. Buck (1989, 1991) and Merski (1998) provide details about the phosphor thermography technique. Horvath (2000) and Berry, et al. (1997a, 1999a, 1999b) are recent examples of the application of phosphor thermography to wind tunnel testing. With this technique, ceramic wind tunnel models are fabricated and coated with phosphors that fluoresce in two regions (red and green) of the visible spectrum when illuminated with ultraviolet light. The fluorescence intensity is dependent upon the amount of incident ultraviolet light and the local surface temperature of the phosphors. By acquiring fluorescence intensity images with a color video camera of an illuminated phosphor model exposed to flow in a wind tunnel, surface temperature mappings are calculated on the portions of the model that are in the field of view of the camera. A temperature calibration of the system conducted prior to the study provides the look-up tables that are used to convert the ratio of the green and red intensity images to global temperature mappings. With temperature images acquired at different times in a wind tunnel run, global heat transfer images are computed assuming one-dimensional heat conduction. The primary advantage of this technique is the global resolution of the quantitative heat transfer data. Such data can be used to identify the heating footprint of complex, three-dimensional flow phenomena (e.g., transition fronts, turbulent wedges, boundary layer vortices, etc.) that are difficult to resolve by discrete measurement techniques. Phosphor thermography is routinely used in Langley's hypersonic facilities because models can be fabricated more quickly and economically than other techniques, and the method provides quantitative global information. Recent comparisons of heat transfer measurements obtained from phosphor thermography to conventional thin-film resistance gages measurements (Merski 1998) and to CFD predictions (Hollis, et al. 1999, Berry, et al. 1999a, Loomis, et al. 1997, Hamilton, et al. 1998 and Horvath, et al. 2000) have shown good agreement.

Flow visualization techniques, in the form of schlieren and oil-flow, were used to complement the surface heating tests. The LaRC 20-Inch Mach 6 Air Tunnel is equipped with a pulsed white-light, Z-pattern, single-pass schlieren system with a field of view encompassing the entire 20-in test core. The LaRC 31-Inch Mach 10 Air Tunnel has recently installed a small 6-inch schlieren system. The schlieren images were recorded with a high-resolution digital camera and video. Surface streamline patterns were obtained using the oil-flow technique. The metal model was spray-painted black to enhance contrast with the white pigmented oils used to trace streamline movement. Surface streamline development was recorded with a conventional video camera, while post-run digital photographs were recorded with a high-resolution digital camera.

Model Description

A sketch of the 33% scale Hyper-X forebody model is shown in Fig. 7. Note that the chines of the forebody model were laterally truncated aft of the first ramp-corner in order to minimize tunnel blockage and to isolate the model within the tunnel test core. A numerically controlled milling machine was used to build the forebody model with a detachable stainless-steel leading edge and interchangeable measurement surface inserts as well as various stainless-steel trip and inlet configurations. Although a majority of the forebody (the strongback) was constructed from aluminum to save weight, the leading edge was machined from stainless steel with a nose radius of 0.010-in to allow replacement if damaged. The length of the leading edge was selected to be 5-in in order to provide for adequate thickness for attachment to the aluminum strongback. The trip station was another 2.418-in aft of the leading edge attachment point (for a total length from the model leading edge of 7.418-in). The interchangeable trip configurations were designed and sized based on the local flow properties at this forebody station. The remaining flat ramp sections were designed to accommodate both Macor and aluminum set of inserts. Macor is a machinable glass ceramic and is a registered trademark of Corning Incorporated. The engine inlet sidewalls were made of stainless steel and were designed to accommodate both open and closed engine cowl door configurations. The open configuration represents the forebody at test point with the engine cowl door in the operating position, although for the wind tunnel model the cowl is removed to provide optical access to the internal flat ramp surface.

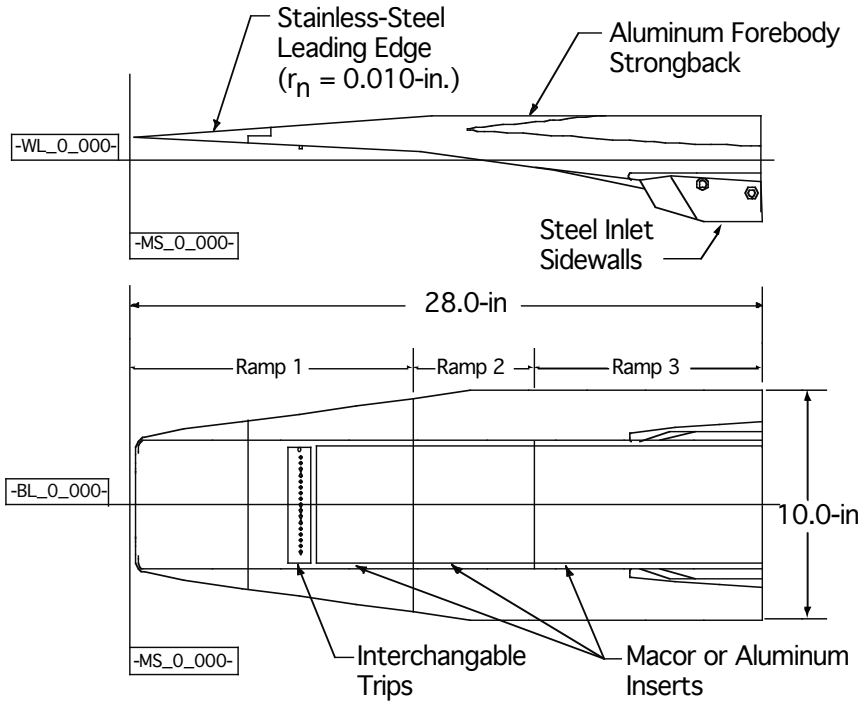

Figure 7. Hyper-X forebody model dimensions.

Normally a cast ceramic process is used to build phosphor thermography models. In this case, precision metal machining was used in lieu of the casting process as a thin high-fidelity leading edge and interchangeable trip configurations were required. As the ramp sections behind the trip location were planar across a majority of the span, 0.25-in thick flat sheets of Macor were used for the phosphor substrate. The Macor substrates were coated with a mixture of phosphors suspended in a silica-based colloidal binder. This coating consisted of a 5:1 mixture of lanthanum oxysulfide (La_2O_2S) doped with trivalent europium and zinc cadmium sulfide (ZnCdS) doped with silver and nickel. The coatings typically do not require refurbishment between runs in the wind tunnel and are approximately 0.001-in thick. The final step in the fabrication process is to apply fiducial marks along the body to assist in determining spatial locations accurately. The fiducial marks used for the present study were the joints between the Macor inserts, which correspond to the location of the ramp angle changes shown in the sketch in Fig. 7.

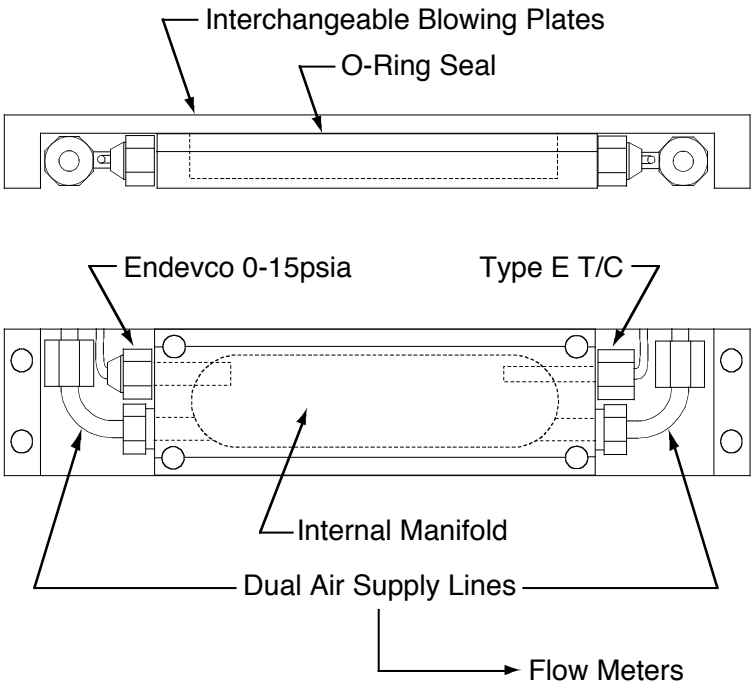

Figure 8. Blowing system assembly details.

The blowing assembly, shown in Fig. 8, was designed to fit within the cavity that held the trip inserts, with consideration of maximizing the internal manifold volume (2.50-in span by 0.750-in wide by 0.309-in deep) while accommodating the instrumentation and air-supply lines. Several interchangeable blowing plates representing the external surface of the assembly were replicated and then further machined to provide the various configurations shown in Fig. 6. The span of the internal manifold (or plenum chamber) limited the width of the blowing configurations to approximately 2-in. The conditions within the plenum were measured with a miniature piezoresistive pressure transducer from Endevco (0-15psia) and a Type E thermocouple with an exposed junction. Pressurized air was provided to the manifold through two supply lines, which were split off a single line through which the total mass flow of the system was measured with various Teledyne Hastings low capacity flow meters. The specific flow meters available for the present study include a HFC-202B with a range up 0.1 standard liters per minute (SLPM), a HFM-200 with a range up to 5 SLPM, and a HFC-203A with a range up to 50 SLPM.

Test Conditions and Data Reduction

Nominal reservoir stagnation and corresponding freestream flow conditions for the present study are presented in Table 2. Flow conditions for the 20-Inch Mach 6 Air and 31-Inch Mach 10 Air tunnels were calculated based on measured reservoir pressures and temperatures and recent unpublished calibrations of the facilities. For the phosphor data, heating rates were calculated from the global surface temperature measurements using the one-dimensional semi-infinite solid heat-conduction equations, as discussed by Buck (1991) and Merski (1998). Based on Merski (1998), phosphor system measurement error is a function of the surface temperature of the model and is typically quoted as 8 to 10% for the 20-Inch Mach 6 tunnel and 7 to 10% for the 31-Inch Mach 10 tunnel, with overall experimental uncertainty of ±15%. The slightly higher uncertainty for the 20-Inch Mach 6 is due to the relatively low temperature driver of the facility that results in lower overall surface temperature rise during a typical tunnel run. As will be shown in subsequent images, a noticeable scatter in the Mach 6 heating images, as compared to similar Mach 10 images is evidence of this increased error. Global heating images are presented in terms of the ratio of heat-transfer coefficients h/h_{ref}, where h_{ref} corresponds to the Fay and Ridell (1958) stagnation-point heating on a sphere with radius 4.0-in (a 1/3rd scale 1-ft radius sphere). Repeatability of heat transfer distributions was generally better than ±4%. For the pressure and mass flow data, the millivolt output from the transducers were converted to engineering units based on a recent calibration of the instruments, and the accuracy is typically quoted as ±15% of full scale.

Discussion of Results

The Hyper-X forebody model has had several entries into the LAL facilities over the years producing numerous runs. Parametrics include the effect of angle-of-attack, Mach number, and Reynolds number for both the passive and active trip configurations with the inlet door simulated in both the open and closed configuration. In order to limit the scope of the present paper, the results to be presented will be for the wind tunnel cases which most closely match the nominal Mach 7 flight case of α = 2-deg, Re_L = 5.6 million with the engine inlet door simulated in the open position. Table 3 provide a comparison of the pertinent parameters in flight to that obtained in the LAL.

No Trip Baseline

Figure 9 is a comparison of the baseline (no trip) results on the Hyper-X forebody between Mach 6 and Mach 10 for the nominal wind tunnel condition of α = 2-deg and Re = $2.2x10^6$/ft. These results suggest a laminar boundary layer over most of the forebody based on comparisons to laminar computations (not shown) and the evidence of separations in the oil-flows. These separated flow regions, which appear relatively two-dimensional over the width of the flat ramps, merge with a separated or low shear region, which runs the length of the chines, to generate a chine vortex emanating from the compression ramp corners. Based on the oil-flows, the surface streamlines indicate flow spillage off the flat ramps, with as little as a third of the surface streamlines at the end of the first ramp being captured by the inlet. These results tend to support the earlier concerns regarding flow separations and mass capture. The baseline phosphor heating images have been scaled to fit within a sketch of the model, in order to correctly align the heating results for comparison to the oil-flows. The heating results show the first two ramps to be laminar, with transition onset occurring on the last ramp. As discussed earlier, natural transition onset just prior to the end of the first ramp minimizes flow spillage and provides a turbulent boundary layer for the inlet. Thus, even in the noisy environment of conventional (non-quiet) hypersonic wind tunnels, forced transition via tripping is required at the nominal conditions.

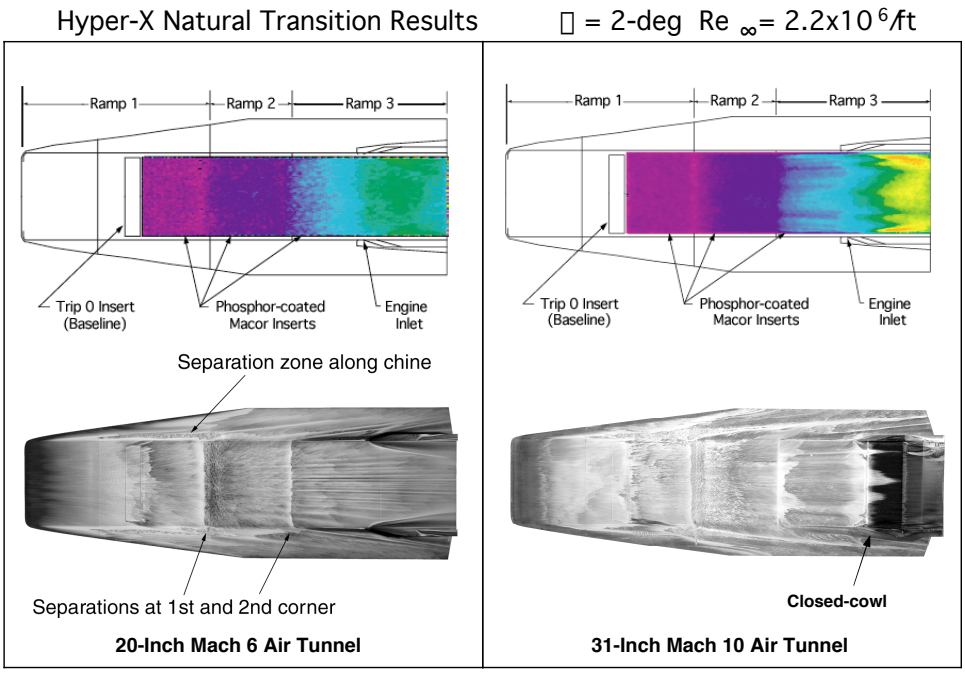

Figure 9. Natural transition results from the Mach 6 and 10 tunnels.

Passive Trips

Figure 10 is a representative comparison of the effect of increased trip height between the passive Trip 1 and 2c configurations in the 31-Inch Mach 10 Tunnel for the nominal condition. As can be seen in the images, the effect of increasing the trip height (k) provides a systematic forward movement of the onset of transition from just inside the inlet to the first ramp. For both trips shown in Fig. 10, the height that just begins to affect

the location of transition onset, the *incipient*[2] value, is k = 0.030-in. By k = 0.060-in for both configurations, a significant forward movement of transition (a *critical* value) onto Ramp 2 is evident. By the largest trip height, k = 0.120-in (the calculated boundary layer thickness at the trip location for Mach 10), the onset of transition has moved ahead of Ramp 2 for Trip 1, while Trip 2c appears to fall behind slightly. Although the Trip 2c configuration is slightly less effective at promoting transition than Trip 1, the minimization of the organized and persistent vorticity into the turbulent regime is desirable in order to reduce the potential heating to the closed cowl. Based on the images, it does not appear that an *effective* value has been reached in the Mach 10 tunnel (as transition is not directly behind the trip location), however comparison of the heat transfer distributions to CFD (not shown) reveal the transition onset is near the trip location for the largest trip.

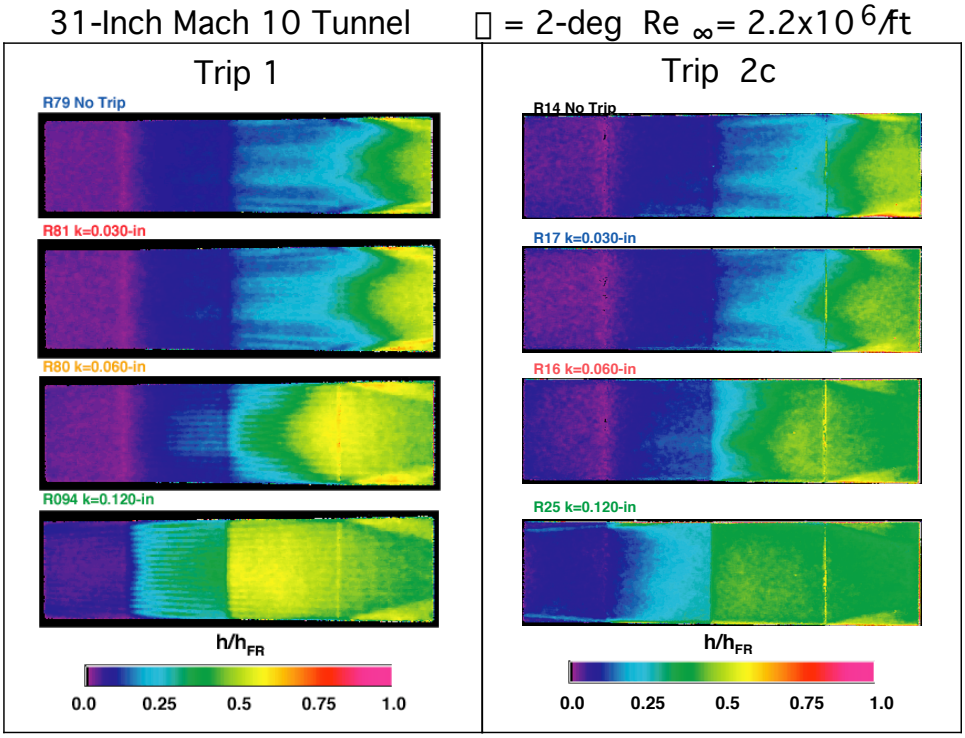

Figure 10. Comparison of passive trip results from the Mach 10 tunnel.

Active Trips

For the current active trip study, the passive roughness elements were replaced with the various blowing module assemblies and the internal manifold pressure and total mass flow of the system were systematically varied and measured. Figure 11 provides an example of the heating and schlieren results obtained for one configuration, the H5 with a single row of 17 spanwise holes (0.020-in D) spaced 1/8-in apart. The internal pressure transducer was used to monitor the static surface pressure during the no blowing runs and typically measured a value of P_2 = 0.08 psi. Typically, twice the local pressure is required to establish sonic flow through the orifices, however the surface pressure near the holes will be slightly higher due to the induced laminar separation that forms ahead of the jet. A manifold pressure of 5 times the static no blowing value produces only slight differences in the schlieren and in the movement of transition. However, as the manifold pressure is increased to roughly 20 times the surface pressure, a greater disturbance is produced in the boundary layer creating a slight shock wave, as noted in the schlieren image, and a corresponding forward progression of transition onto the second ramp. Increasing the manifold pressure to 80 times the static pressure generates an even stronger jet shock and movement of transition to the first ramp. For the highest pressure

[2] Note that the terminology used here is similar to the definitions of Bertin, et al. (1982). *Incipient* identifies the maximum roughness height that has little effect on the onset of transition. *Critical* identifies the roughness height that first begins to move transition rapidly towards the nose. *Effective* identifies the minimum roughness height that establishes transition onset just downstream of the roughness element.

case shown, $P/P_2 = 250$, a clear Mach disk, indicating the jet penetration height, is revealed in the schlieren at the top of the jet that is approximately the same height as the calculated boundary layer thickness, which moves the jet induced shock further away from the body and forces the separation region far forward on the model. Note that for this case, transition movement seems to have stabilized just behind the trip location, and in fact the overall heating levels in the turbulent region seems to have been reduced slightly.

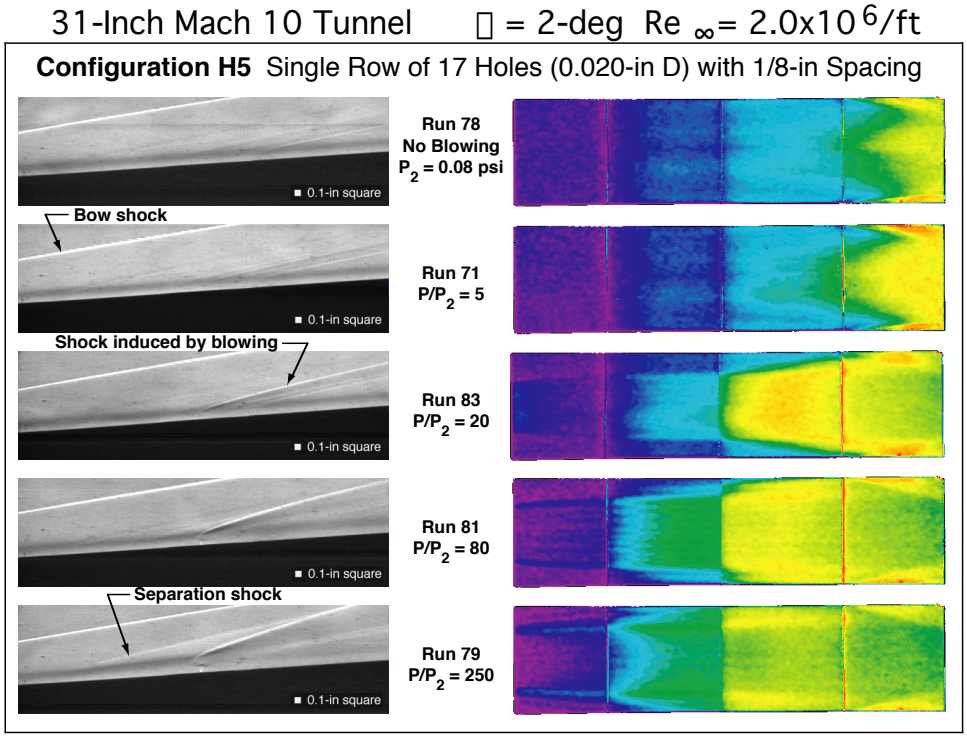

Figure 11. Sample active trip results from Mach 10 tunnel.

To systematically interpret the transition onset locations, the heating images were used to extract a spanwise array of heating distributions along the streamwise direction, which were then averaged (to minimize scatter) and compared to a baseline (no blowing) case. The transition onset locations were identified by the departure of more than 10% above the laminar baseline heating distribution, as indicated and marked in Fig. 12. When analyzed in this manner, the onset of transition is evident on Ramp 1 for the highest pressures, although that fact is not obvious by trying to interpret the heating images. The pressure range measured during the present study was adequate for providing the same amount of transition movement observed in the previous passive trip investigation and shown in Fig. 10. For the lowest blowing case, with a manifold pressure of just 5 times the static measurement, the onset of transition appears to move slightly forward of the natural location of x/L=0.5 (approximately the inlet station) to x/L=0.41. By doubling the pressure ratio to 10, transition onset is observed to jump ahead onto the second ramp at x/L=0.31. Subsequent doublings of the pressure only produces a slight but steady forward movement of transition on the second ramp until a pressure ratio of 80 brings onset to the ramp corner (x/L=0.26). By increasing the plenum pressure once again to now 160 times the measured static pressure, transition is seen to jump ahead to the first ramp at an x/L=0.22. No further forward movement of transition is observed past this location as the pressure is increased further. In fact while the size of the jet observed in the schlieren continues to increase as the plenum pressure increases, along with the induced shock and separation, the transition movement is clearly optimized for the H5 configuration for a manifold pressure of 160 times the measured static pressure. Further increases to the manifold pressure only serve to reduce the measured heating levels as shown in the distributions in Fig. 12 and comparisons of the images of Fig. 11. It is interesting to note that the transition movement is greatly influenced by the ramp corners, with onset typically jumping forward close to the next corner region as the tripping effectiveness is increased. How much the discrete ramps affect the actual effectiveness of any given trip configuration is unclear and may warrant further investigation.

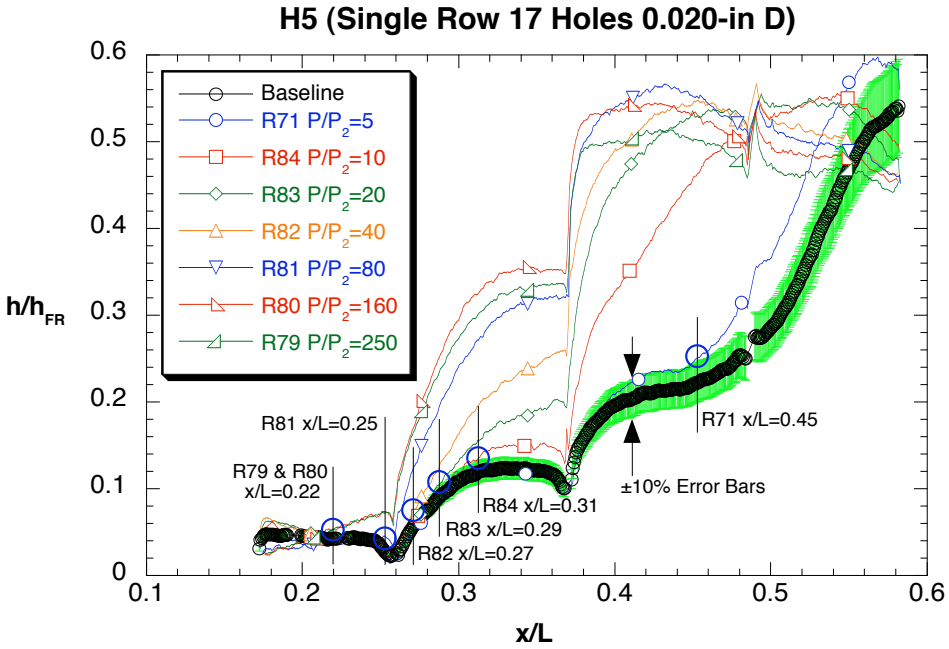

Figure 12. Typical averaged heat transfer distribution for locating transition onset for the Mach 10 data.

Based on the Ames compressible flow tables the minimum pressure ratio (P/P_2) across the surface that is required to establish sonic flow through the orifices is 1.89, neglecting for the moment the potential flow separation region ahead of the sonic orifice that would increase the local pressure. For laminar conditions, jet induced flow separations would augment the local pressure by a factor of roughly 2 or more, based on discussions by Spaid and Cassel (1973). The rough rule of thumb used here is that a P/P_2 of 4 is an indication that the flow within the holes or slots is sonic. For pressure ratios above this value, the sonic jets would expand farther out into the boundary layer increasing the jet penetration height and separation regions. Figure 13 shows the present results from the 31-Inch Mach 10 Tunnel for measured transition onset as a function of the plenum-to-static pressure ratio for all configurations tested, indicating that typically a manifold pressure of 5 times the surface static pressure is required to move the transition point appreciably away from the natural position of x/L=0.5. Based on the schlieren results shown in Fig. 11, P/P_2=5 produces just enough of a disturbance in the boundary layer to establish a very subtle shock emanating from the jet, which would suggest that the Mach disk is very close to the wall. To get significant movement of transition to nearly the effective point (at or near the trip location), a pressure ratio on the order of 10 times the sonic limit (approximately P/P_2=40) is required. As can be seen in Fig. 13, the best performer, in terms of the most transition movement for the lowest pressure was the saw tooth configurations. The S2, both with and without the backing plates to block off sections of the saw tooth slot, was able to get nearly effective movement of transition for pressure ratios of approximately 20 to 40. The next best was configuration H5, a single row of 17 0.020-in holes, spaced 1/8-in apart, which had the best transition movement for the lower manifold pressure cases, but surprisingly tapered off by the higher pressures. Next, the straight slot configurations had systematic forward movement of transition that approached the effective limit at a pressure ratio near 100. Surprisingly, the addition of the BP4 backing plate to the S1 did not affect the results significantly. Conventional wisdom would suggest that the straight slot would generate a two-dimensional disturbance that would be far less effective at promoting transition and the backing plates were intended to introduce three-dimensionality to this configuration. The porous configurations, P1 and P2, were able to achieve effective tripping for a pressure ratio of 160. The results shown in Fig. 13 suggest that the higher the mass flow for a given configuration the better the performance as the S2 has the largest total exit area and thus requires the most flow to maintain the set plenum pressure. The trends observed in the Mach 6 tunnel for the same set of configurations is that the saw tooth and larger hole configurations performed the best for a given plenum pressure. Figure 14 provides a comparison of the shock system around both passive and active trip configurations for representative cases in which the heating results indicated that the transition onset results were nearly effective. The two passive trip

results represent the same cases shown earlier, the Trip 1 and 2c configurations for the largest trip height, k=0.120-in. The calculated boundary layer thickness for the wind tunnel conditions shown was δ = 0.125-in, shown in Table 3. The observed boundary layer edge from the schlierens, as interpreted by the darker band above the surface, essentially matches the trip height. The two active trip cases shown correspond to the best performers, the S2 and H5 configurations, for the minimum pressure ratios required to obtain effective tripping, P/P_2 of 40 and 160, respectively. The observed jet penetration height for both active examples was smaller than the boundary layer edge, roughly a h/δ of 0.5 for S2-BP7 and 0.75 for H5, although the subsequent jet shock and flow separations were larger than the passive cases. The jet penetration height alone is not directly analogous to the passive trip height, nor is the pressure ratio across the surface a good indication of trip effectiveness.

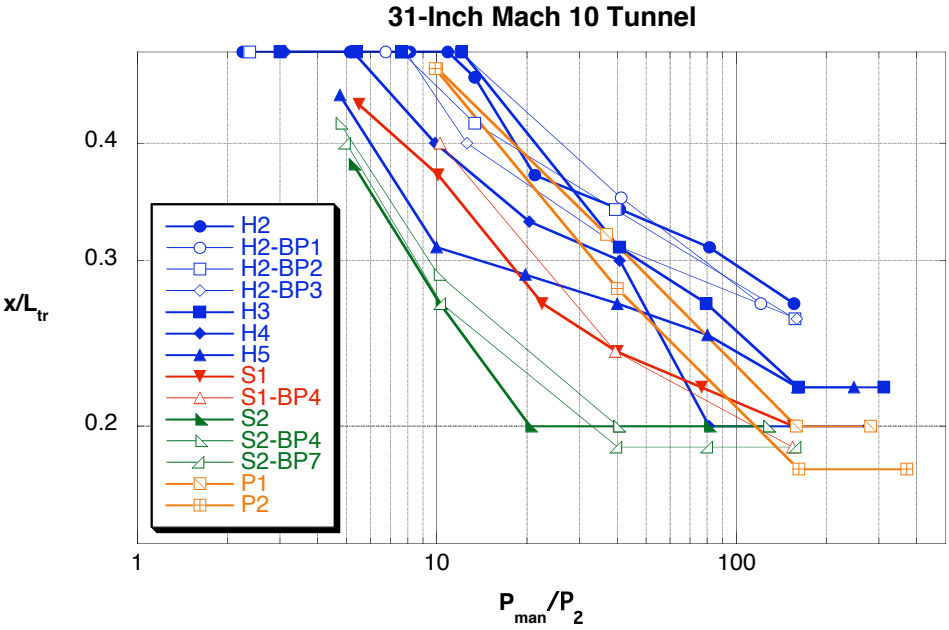

Figure 13. Comparison of transition location as a function of manifold pressure for all configurations tested.

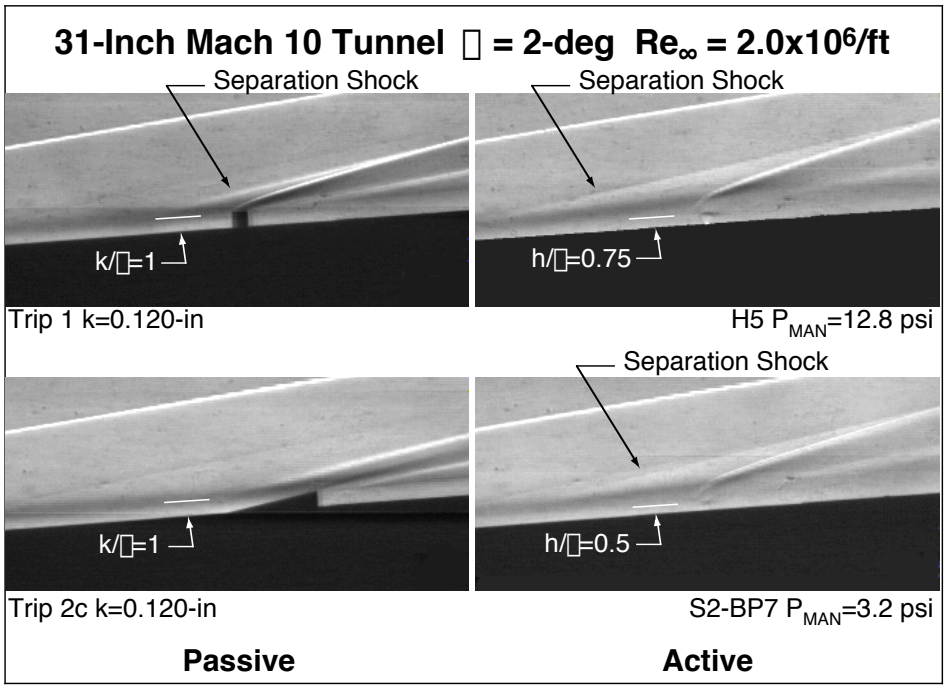

Figure 14. Comparison of flowfield and shock structure between passive and active trips for effective results.

Conclusions

An experimental investigation of boundary layer trip effectiveness on a 33% scale Hyper-X forebody model has been conducted in the 20-Inch Mach 6 Air Tunnel and the 31-Inch Mach 10 Air Tunnel. These facilities provided an adequate range of the Mach numbers and length Reynolds numbers to allow simulation of Mach 7 flight conditions. Phosphor thermography was used to provide heat transfer images and distributions, which was used to monitor the movement of transition onset locations for a variety of active and passive boundary layer tripping elements. The aeroheating results were complemented with oil-flow images that provided surface streamline information and schlieren images that provided shock system details. The passive trip results have previously been used to select a final trip configuration and height for the Mach 7 flight vehicle.

For the most recent experimental study, fourteen blowing configurations were screened and the results indicated that all were adequate for providing transition onset movement. Pressure ratios across the model surface as low as 5, which barely ensures that sonic conditions are maintained through the minimum area, or throat, were adequate for moving transition away from the natural transition location. To move transition onset to the trip location, thereby providing an effective trip, pressure ratios of 40 or higher were required. The saw tooth slot (S2) provided the best movement of transition for the smallest pressure ratio across the model surface, while the H5 configuration (with the larger hole diameter arraigned in a single row) was the best of the round hole concepts. The configurations with the larger throat areas typically performed better and with smaller jet penetration heights, indicating that the mass flow of the configurations may be as important as the pressure ratio when trying to relate these trends to the passive results.

Acknowledgment

This experimental effort was accomplished with the help of many dedicated individuals, a few of which are mentioned here. The model was built with the help of William Kimmel, Kevin Meidinger, Greg Draughon, Mike Powers, Mark Griffith, and Jim Bartlett. Mark also came to the rescue with his assistance in quickly repairing the model during a recent tunnel entry. The LAL testing was accomplished with the support of Paul Tucker, Johnny Ellis, Rhonda Murphy, Henry Fitzgerald, Tony Robbins, Grace Gleason, Bert Senter, Kevin Hollingsworth, Glenn Bittner, and Ron Merski.

References

Berry SA, Auslender AH, Dilley AD, and Calleja JF. 2001. Hypersonic Boundary Layer trip Development for Hyper-X. *J. Spacecr. Rockets 38(6): 853-864*

Berry SA, DiFulvio M, Kowalkowski MK. 2000a. Forced Boundary Layer Transition on X-43 (Hyper-X) in NASA LaRC 31-Inch Mach 10 Air Tunnel. *NASA/TM-2000-210315*

Berry SA, DiFulvio M, Kowalkowski MK. 2000b. Forced Boundary Layer Transition on X-43 (Hyper-X) in NASA LaRC 20-Inch Mach 6 Air Tunnel. *NASA/TM-2000-210316*

Berry SA, Horvath TJ, DiFulvio M, Glass C, Merski NR. 1999a. X-34 Experimental Aeroheating at Mach 6 and 10. *J. Spacecr. Rockets 36(2): 171-178*

Berry SA, Horvath TJ, Hollis BR, Thompson RA, Hamilton HH. 1999b. X-33 Hypersonic Boundary Layer Transition. *AIAA Paper 99-3560*

Berry SA, Horvath TJ, Roback VE, Williams GB. 1997a. Results of Aerothermodynamic and Boundary-Layer Transition Testing of 0.0362-Scale X-38 (Rev. 3.1) Vehicle in NASA Langley 20-Inch Mach 6 Tunnel. *NASA TM-112857*

Bertin JJ, Hayden,TE, Goodrich WD. 1982. Shuttle Boundary-Layer Transition Due to Distributed Roughness and Surface Cooling. *J. Spacecr. Rockets 19(5):389-396*

Buck GM. 1989. Automated Thermal Mapping Techniques Using Chromatic Image Analysis. *NASA TM 101554*

Buck GM. 1991. Surface Temperature/Heat Transfer Measurement Using A Quantitative Phosphor Thermography System. *AIAA Paper 91-0064*

Calleja JF. 2000. Boundary Layer Transition Experiments on a One-Third Scale Hyper-X Forebody Model at Mach 7 and 10. *GASL Technical Report No. 382*

Dilley AD. 1996. Hyper-X Trip Sizing and Preliminary Drag Estimates. *Hyper-X Technical Note 96HN0064, NAS1-19864*

Fay JA, Ridell FR. 1958. Theory of Stagnation Point Heat Transfer in Dissociated Air. *J. Aerosp. Sci.* 25(2):73-85,121

Hamilton HH, Berry SA, Horvath TJ, Weilmuenster KJ. 1998. Computational/ Experimental Aeroheating Predictions for X-33 Phase II Vehicle. *AIAA Paper 98-0869*

Hollis BR, Horvath TJ, Berry SA, Hamilton HH, Alter SA. 1999. X-33 Computational Aeroheating Predictions and Comparisons with Experimental Data. *AIAA Paper 99-3559*

Horvath TJ, Berry SA, Merski NR, Fitzgerald SM. 2000. X-38 Experimental Aerothermodynamics. *AIAA Paper 2000-2685*

Lau KY, Vaporean CN. 1992. Parametric Boundary Layer Transition Study for NASP-like Configuration Using Linear Stability Analyses. *Presented at the National Aerospace Plane Mid-term Technology Review, Monterey CA, paper number 283.*

Loomis MP. Venkatapathy,E, Davies CB, Campbell CH, Berry SA, Horvath TJ, Merski NR. 1997. Aerothermal CFD Validation and Prediction for the X-38 Program. *AIAA Paper 97-2484*

McClinton CR, Holland SD, Rock KE, Englund WC, Voland RT, Huebner LD, Rogers RC. 1998. Hyper-X Wind Tunnel Program. *AIAA Paper 98-0553*

Merski NR. 1998. Reduction and Analysis of Phosphor Thermography Data with the IHEAT Software Package. *AIAA Paper 98-0712*

Micol JR. 1998. Langley Aerothermodynamic Facilities Complex: Enhancements and Testing Capabilities. *AIAA Paper 98-0147*

Miller CG. 1990. Langley Hypersonic Aerodynamic/Aerothermodynamic Testing Capabilities - Present and Future. *AIAA Paper 90-1376*

Rausch VL, McClinton CR, and Crawford JL. 1997a. Hyper-X: Flight Validation of Hypersonic Airbreathing Technology. *ISABE Paper 97-7024*

Rausch VL, McClinton CR, Hicks JW. 1997b. NASA Scramjet Flights to Breath New Life into Hypersonics. *Aerospace America 35(7): 40-46*

Spaid FW, Cassel LA, 1973. Aerodynamic Interference Induced by Reaction Controls. AGARD-AG-173

Stetson KF, Thompson ER, Donaldson JC, Siler LG. 1984. Laminar Boundary Layer Stability Experiments on a Cone at Mach 8, Part 2: Blunt Cone. *AIAA Paper 84-0006*

Stone DR, Cary AM. 1972. Discrete Sonic Jets Used as Boundary-Layer Trips at Mach Numbers of 6 and 8.5. *NASA TN D-6802*

Table 1: Hyper-X trip screening tests in NASA facilities.

Year	Tunnel	Test	Occupancy Dates	Runs	Description
1997	31-In M-10	338	Aug 14 – Aug 29	1-76	Phosphor
1997	20-In M-6	6755	Sept 2 - Sept 5	1-61	Phosphor and schlieren
1997	31-In M-10	338	Sept 30 - Oct 20	77-170	Phosphor and oil-flow
1998	20-In M-6	6768	Mar 30 – Apr 2	22	Oil-flow
1998	31-In M-10	346	Apr 6 - Apr 10	1-20	Oil-flow
1998	31-In M-10	349	Sept 3 - Sept 8	1-25	Phosphor with new trip
1998	31-In M-10	351	Sept 16 - Sept 18	1-19	Phosphor on closed cowl
1999	HYPULSE		Feb 23 – Mar 26	1-28	Thin-film and schlieren
1999	20-In M-6	6791	Aug 10	1-10	Phosphor with new trip
1999	20-In M-6	6793	Sept 15 - Sept 17	1-11	Phosphor w/ leading edge roughness
2002	20-In M-6	7842	July 12 – July 26	1-79	Blowing with Phosphors
2002	20-In M-6	6847	Dec 6 – Dec 16	1-42	Blowing with oil-flow
2003	31-In M-10	385	Oct 22 – Nov 18	1-152	Blowing with Phosphors

Table 2: Nominal tunnel flow conditions.

Tunnel	Re_∞(x10^6/ft)	M_∞	P_{t1} (psi)	T_{t1} (°R)	H_{t1}(BTU/lbm)	P_{t2}(psi)
20-In Mach 6	2.2	6.0	125.5	906.6	218.2	3.8
31-In Mach 10	2.2	9.9	1451.7	1808.1	454.8	4.5
HYPULSE	1.4	7.31	1994.3	3951.0	1079.4	18.6

Table 3: Calculated boundary layer parameters at the trip location.

Tunnel or Flight	M_∞	Re_∞(x10^6/ft)	δ (in)	M_e
20-In Mach 6	6.0	2.2	0.081	3.1
31-In Mach 10	9.9	2.2	0.125	4.4
HYPULSE	7.3	1.4	0.075	4.2
Mach 7 Flight	7.0	0.9	0.180	3.4
Mach 10 Flight	10.0	0.6	0.283	4.5

Nomenclature

M Mach number
Re unit Reynolds number (1/ft)
Re_L Reynolds number based on body length
Re_δ momentum thickness Reynolds number
R_n nose radius (in)
α model angle of attack (deg)
δ boundary layer thickness (in)
P pressure (psi)
T temperature (R)
x longitudinal distance from the nose (in)
y lateral distance from the centerline (in)
z height above the waterline (in)
L reference length of vehicle at the model scale (48.00 in)
h heat transfer coefficient (lbm/ft^2-sec), $=q/(H_{aw} - H_w)$ where $H_{aw} = H_{t2}$
h_{FR} reference coefficient using Fay-Ridell calculation at stagnation point of a sphere
q heat transfer rate (BTU/ft^2-sec)
H enthalpy (BTU/lbm)
k roughness element height (in)
h jet penetration height (in)

Subscripts

∞ freestream static conditions
t1 reservoir conditions
t2 stagnation conditions behind normal shock
aw adiabatic wall
e conditions at edge of the boundary layer
man conditions within the manifold
w model surface
inc incipient
cr critical
eff effective
tr location of transition onset
2 local static conditions